JOURNAL OF MATERIALS SCIENCE **40** (2005) 6113–6120

Micro-indentation creep of porous nanocrystalline metallic and composite compacts

K. A. PADMANABHAN*†
Institute of Nanotechnology,Research Centre Karlsruhe, P.O. Box 3640, D 76021 Karlsruhe, Germany
E-mail: kapsp@uohyd.ernet.in, ananthaster@gmail.com, kap19452002@yahoo.co.in

P. MONDAL
Institute of Materials Science, Darmstadt University of Technology, Petersenstr. 23, D 64287 Darmstadt, Germany

H. HAHN
Institute of Nanotechnology,Research Centre Karlsruhe, P.O. Box 3640, D 76021 Karlsruhe, Germany; Institute of Materials Science, Darmstadt University of Technology, Petersenstr. 23, D 64287 Darmstadt, Germany

Published online: 8 September 2005

Experimental observations concerning the time dependent variation in the room temperature microhardness of porous compacts of nanocrystalline Palladium are presented. These data and the earlier findings on the elevated temperature response of compacts of nanocrystalline composites Fe-63 vol% TiN and Ni-58 vol% TiN are interpreted as due to power law creep. The equations developed are validated using the experimental results.

1. Introduction

Mechanical behaviour of nanostructured (n-) materials is examined in many papers and is also discussed in several reviews (see, for example, refs. [1–6]). Obtaining large specimens through the powder metallurgical route for mechanical testing has been difficult. The processing route/processing sequence strongly affects the mechanical response. In a compact grain/pore size and shape, their distributions, other flaws/defects and their distribution, nature of the bond present in the material, impurity level, second phases/dopants, microstructures on a variety of length scales, internal stresses, surface condition, externally applied stresses, duration of stress application and temperature of deformation all influence the mechanical properties.

For structural applications, compacts of (near-) full density are needed. But a porous microstructure is desired for some other applications, e.g., catalytic [7], orthopaedic/dental implant [8] applications. That means that it is often necessary to prepare compacts of different relative densities out of the same material powders. To achieve this, an understanding of the changes in the mechanical response of compacts with the relative density should be available. Evidently, the mechanical response of a (near-) fully dense compact should be used as the standard/base line against which comparisons are ultimately made. But, no quantitative studies are available at present that correlate the mechanical response of nanocrystalline porous compacts with that of fully dense compacts. Such studies are common in the literature on powder metallurgy of materials of conventional grain sizes (see, for example, refs. [9–11]). It is known from those investigations that elastic properties like the shear modulus, the Poisson ratio, plastic/viscous properties like yield/tensile strength, ductility, creep behaviour etc. change with the relative density. This has a bearing on the processing characteristics, the conditions of processing, the load bearing capacity of the resultant component and so on. If nanostructured materials are to be exploited on a large scale, a data-base of this kind has to be generated.

The relative density of a compact is found from a comparison of the weight and volume of that compact with those of a fully dense compact. Such a comparison, however, gives only an idea about the total pore volume. But at the local level, the behaviour can be different in two compacts of equal relative density, if the size and shape distributions of pores are different.

In this paper room temperature microhardness variations in n-Pd compacts of different relative densities, which are regarded as specimens pertaining to a model system, are reported at different locations as a function

*Author to whom all correspondence should be addressed.
†*Present Address*: School of Physics,University of Hyderabad, Hyderabad, 500 046, India.
0022-2461
DOI: 10.1007/s10853-005-3171-5

of load application. These results as well as the earlier experimental results of Ogino *et al.* [12] concerning microhardness variations in nanocrystalline Fe-63 vol% TiN and Ni-58 vol% TiN composites as functions of time of load application and test temperature, were analysed using equations developed based on an assumption that the time dependent variation in microhardness is due to creep flow. We believe this to be a reasonable assumption because even in fully dense high melting materials like n-Ni and nano-Ni-W alloy creep flow was present at room temperature [13, 14]. It is known [15] that, if anything, deformation becomes easier as the microstructure becomes less dense.

But there are also situations where the nanocrystalline material is brittle at room temperature, e.g., nanocomposites of high melting phases, nanostructured materials contaminated by brittle oxides etc. [1–6]. Therefore, it appears reasonable to suggest that creep flow in nanocrystalline materials at room temperature can be expected only under conditions that favour creep flow, e.g., in single phase materials, materials of relatively low melting points, factors and dopants that enhance the diffusivity of materials etc. Needless to say in most—if not all—nanostructured materials, the creep effects become stronger with increasing temperature of deformation.

This work is at the level of phenomenology. A more detailed investigation dealing with local microstructure changes accompanying plastic/creep flow will be presented in the future.

2. Experimental

Pure nanocrystalline Pd powders were synthesized from coarse grained Pd nuggets of 99.999% purity using the gas condensation technique [16]. The machine used for this purpose was built, according to our design, by HBI GmbH, Germany. A tungsten boat was used for heating and evaporating Pd in an ultra high vacuum (UHV) chamber at a low helium gas pressure of 10 mbar. Metal clusters, condensed on a rotating cold finger filled with liquid nitrogen, were scraped and transferred under UHV conditions to a compaction unit. The powders were compacted at temperatures ranging from 20 to 300°C and pressures that lay between 400 MPa and 1 GPa to discs of 9.5 mm diameter and thickness varying from 0.15 to 1.00 mm. In all 8 compacts were made. Average relative density, ρ_{av}, of each compact was calculated from the mass and the measured volume of the sample. The average density of the compacts ranged from 58 to 94% of the theoretical density. X-ray diffraction was used to check the phase purity on a Siemens D 5000 X-ray diffraction unit. Sample purity was checked by energy dispersive X-ray analysis on an EDAX CDU Leaf Detector attached to a Philips XL 30 FEG machine. Grain size of the compacts was determined using Cu radiation in a Siemens D-5000 diffractometer working in the Bragg-Brentano geometry. Average grain size was calculated from the broadening of the Bragg peaks in the XRD patterns using the Scherrer formula [17]. As this formula does not take into account the rms strain, to ensure the reliability of the values obtained, grain size, microstructure and grain size distribution were also characterised by high resolution scanning electron microscopy (HRSEM) on a Philips XL 30 FEG machine and atomic force microscopy (AFM) (Thermo Microscopes CP). The average grain sizes obtained by the three methods were in good agreement. Fig. 1, obtained using AFM, in which the average grain size and grain size distribution are indicated, is an example.

Vickers microhardness values at different locations in each of the 8 compacts were obtained on a microhardness tester of Helmut Fischer make capable of applying a constant load for different periods of time. As this instrument works on the principle of magnetostriction, internal heating may introduce significant errors in the readings after some time. Therefore, the maximum permissible time for making *reliable* measurements at the load chosen for the present experiments (=1 N) was found out first using a standard specimen. For this purpose, a coarse grained alumina specimen of bimodal grain size distribution (the mean values were 8 μm and 21 μm) was chosen as the standard. In this material, at room temperature *no creep effects* are expected and so the microhardness should be independent of the time of load application. Fig. 2 presents the findings. It is clear that the instrument errors affect the results for times of load application greater than 50 s. Thus, in the n-Pd compacts if the microhardness varies with time at a load of 1 N at a time interval of less than 50 s, this should be regarded as a genuine creep effect. This upper limit of 50 s is also beneficial for two other reasons: (a) at longer time intervals, perceptible grain growth could be present in Pd [18]; (b) this short time limit will allow a comparison between the response during a short duration test and that obtained over a long period of time [12] (In those tests [12], unlike the present machine that works on the principle of magnetostriction, a conventional Vickers microhardness tester was used on which tests of long duration could be carried out without the introduction of artefacts/unreliability in the results.). In view of the above, the time of load application in the microhardness tests was kept below 50 s. Fig. 2 reveals

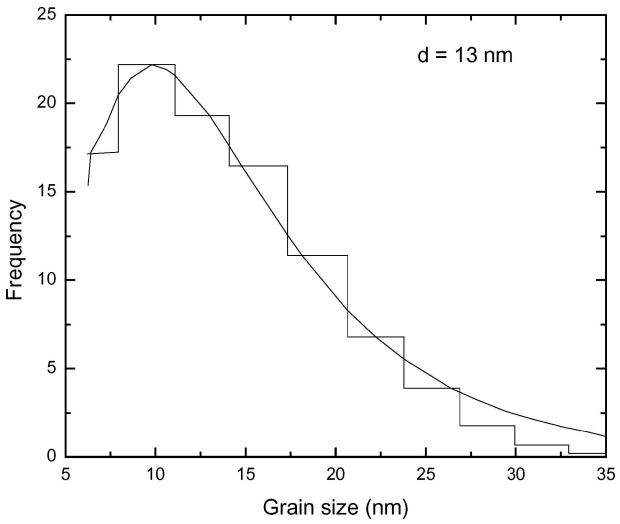

Figure 1 Grain size - frequency distribution in a Pd compact of average grain size ≈13 nm obtained using an atomic force microscope and the software available with the equipment.

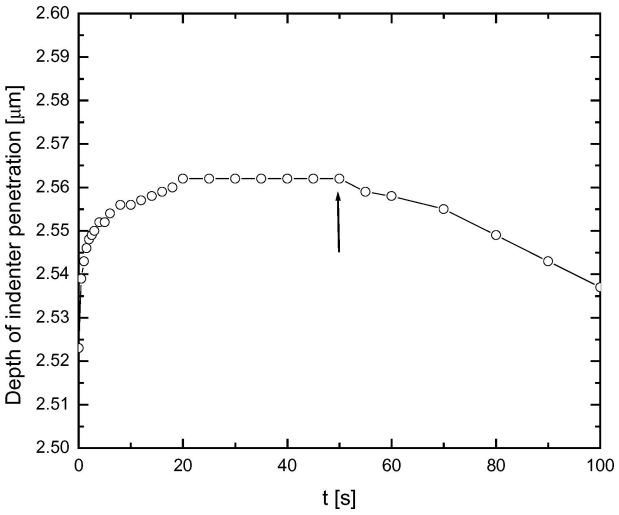

Figure 2 Depth of indenter penetration-time of load application relationship for a coarse grained alumina standard sample. Load applied = 1 N.

in addition that the microhardness reaches its steady state/maximum value within a very small fraction of the time of load application. This result is consistent with the assumption that the microhardness test may be analysed as a quasi-steady state process. A software installed in the microhardness tester gave at the onset point of the steady state the values of the microhardness (H) and the corresponding Young's modulus (E).

The procedure used to obtain the experimental microhardness—time of load application—test temperature curves for Fe-63 vol% TiN and Ni-58 vol% TiN nanocomposites, which are also examined in Section 4, are given elsewhere [12].

3. A phenomenological analysis of micro-indentation creep in nanostructured materials

The microindenter has a non-uniform cross-section. The slant side often consists of flat faces, which will introduce discontinuities in the stress and strain fields. Material flow opposite to the direction of indenter penetration gives rise to frictional forces. To simplify the analysis, following Li *et al.* [19] two assumptions are made: (a) the penetration of a compact by a microindenter is treated as a quasi-steady state process, and (b) the microhardness—time relationship for a Vickers diamond pyramid-conical indenter is assumed to differ from that for a simple conical indenter by an *unknown* constant. The latter approximation amounts to ignoring the discontinuities in the stress distribution so that integration and differentiation are possible.

3.1. Time-dependent microhardness variation

For certain functional applications, it may be necessary to produce compacts of less than 100% theoretical density. Such compacts will be reasonably homogeneous and practically useful. The aim is to obtain an expression for hardness as a function of time of load application for such materials in a microhardness test, $H = H(t)$. We visualise three possibilities.

Case 1: This is a trivial solution for which $H(t) = H_0$, where H_0 is the microhardness at the commencement of load application. Such a situation is encountered when there is no creep effect in the material under the given experimental conditions, e.g., a nanocrystalline ceramic compact subjected to a microhardness test at room temperature. In this case, the microhardness remains constant throughout a test.

Case 2: A large subcutaneous pore/cavity is present right below the point at which indenter penetration takes place or the compaction in the vicinity of the site of indentation is extremely inhomogeneous. In this case the microhardness variation with time will not be continuous, but the hardness will vary at different rates at different times of load application. (There will be discontinuities in the relationship.) A general mathematical treatment of this problem is not possible and materials with such microstructures will be unusable in service.

Case 3: This is the useful case discussed above. The following analysis is restricted to this case.

For (a pyramid-) conical indenter [19]

$$H = (W/\pi a^2) \tag{1}$$

where H is the microhardness, W is the load applied and 'a' is the instantaneous radius of the indentation. H is related to the uniaxial yield stress, σ, as $H = C_1\,\sigma$, where C_1 is an *unknown* constant for a nanocrystalline material. From Equation 1,

$$\dot{a}/a = -(\dot{H}/2H) \tag{2}$$

where the 'dot' represents a time derivative.

Following Li *et al.* [19], the radial velocity is assumed to vary linearly with $\dot{a}$. As the cone angle of the indenter is fixed, $(\frac{h}{a}) =$ constant, the tangent of the semi-angle of the cone. Therefore, $h \propto a$; $\dot{h} \propto \dot{a}$ By definition, the mean strain rate of deformation,

$$\begin{aligned} \dot{\varepsilon} &= \tfrac{\dot{h}}{h},\ Or \\ \dot{\varepsilon} &= C_2\left(\tfrac{\dot{a}}{a}\right) \end{aligned} \tag{3}$$

where C_2 is another unknown constant. From Equations 2 and 3

$$\dot{\varepsilon} = -C_3(\dot{H}/H); C_3 = (C_2/2) \tag{4}$$

In view of the creep equation $\dot{\varepsilon} = K_1\sigma^N$ (K_1 and N are constants under isostructural, isothermal conditions [20]), the relation $H = C_1{\cdot}\sigma$ and Equation 4,

$$-(\dot{H}/H) = C_4 \cdot H^{\mathrm{N}}; \quad C_4 = 1/\left(C_3 \cdot C_1^{\mathrm{N}}\right) \tag{5}$$

From Equation 5

$$-(dH/H^{\mathrm{N}+1}) = C_4.dt \tag{6}$$

This integrates to give

$$(1/H^N) = C_5 t + C_6; \quad C_5 = (C_4 \cdot N) \tag{7}$$

with t the time of load application. The constant of integration C_6 is obtained as equal to $\left(1/H_{\max}^{\mathrm{N}}\right)$ from the initial condition that at $t = 0$, H equals its initial/maximum value, $H_{\max}$. Therefore,

$$-N \ln H = \ln[1/H_{\max}^{N}(C_7 t + 1)];$$
$$C_7 = (C_5 H^{N}{}_{\max}) \tag{8}$$

$$= -N \ln H_{\max} + \ln(C_7 t + 1) \tag{9}$$

As $N = (1/m)$, where m is the strain-rate sensitivity index, Equation 9 is transformed into

$$H = H_{\max} \cdot e^{-m \ln(C_7 t + 1)} \tag{10}$$

On first order approximation,

$$H \approx H_{\max} - A \ln(Bt + 1);$$
$$A = H_{\max} \cdot m; \quad B = C_7 \tag{11}$$

Equation 11 describes the variation of hardness with time in a microhardness test. This expression contains a single fitting parameter, B.

3.2. Activation energy for rate controlling flow

As the temperature dependence of deformation follows the Maxwell-Boltzmann relationship, from Equation 5

$$-(\dot{H}/H) = A_1 (H/H_c)^{\mathrm{N}} \exp(-Q/RT) \tag{12}$$

where A_1 is a grain-size dependent constant (with a dimension of time^{-1}), which has absorbed the thermal vibration frequency of 10^{13} s^{-1}, Q the activation energy for the rate controlling process, R the gas constant, T the absolute temperature of deformation and H_c is a reference hardness value (chosen as applicable to the domain of interest) introduced to ensure dimensional consistency. Therefore,

$$-(\dot{H}/H) = A_2 H^N \exp(-Q/RT); \quad A_2 = (A_1/H_c^N) \tag{13}$$

Depending on the range covered in the experiments in the $\{-(\dot{H}/H) - H - T\}$ space, it may be convenient to determine Q either by plotting $\ln(-\dot{H}/H)$ against $1/T$ at a constant hardness value H_1 or $\ln H$ against $1/T$ at a constant $-(\dot{H}/H)$ value [20]. From Equation 13 it follows that

$$Q = -\{\text{slope of the } \ln(-\dot{H}/H) \text{ vs. } (1/T) \text{ plot at } H = H_1\} \cdot R \tag{14}$$

TABLE I Young's modulus-microhardness-time dependence relationships in *n*-Pd Compacts of different densities

S.no.	Av. grain size (nm)	ρ_{av} (%)	$E_{initial}$ (GPa)	$H_{initial}$ (H_{max}) (MPa)	H_{min} (MPa)	m	A (MPa)	B (s^{-1})	($H_{max} \cdot m$) (MPa)	$\lvert A - H_{max} \cdot m \rvert$ /A (% error)*
1	62	94	67.601	1326	1266	0.01	12.53	2.35	13.26	6
2	62	94	76.600	1605	1520	0.01	17.70	2.26	19.26	9
3	62	94	68.199	1294	1218	0.01	16.53	1.62	18.12	10
4	11	63	10.000	519	473	0.02	10.44	1.59	11.42	9
5	11	63	7.131	379	344	0.02	6.22	1.81	6.82	10
6	11	63	5.210	254	233	0.02	4.90	1.46	5.33	9
7	21	90	4.651	249	238	0.01	2.17	2.70	2.24	3
8	21	90	12.400	490	472	0.01	5.43	2.83	5.49	1
9	21	90	8.510	407	387	0.01	4.35	1.97	4.48	3
10	21	90	3.041	157	149	0.01	1.72	1.70	1.88	9
11	21	90	2.271	131	126	0.01	1.02	1.56	1.05	3
12	11	71	26.199	1428	1298	0.02	26.17	2.95	28.56	9
13	11	71	34.700	1546	1389	0.02	31.42	2.88	34.01	8
14	11	71	3.831	177	170	0.01	1.49	2.04	1.59	7
15	11	71	8.479	379	362	0.01	3.19	4.67	3.41	7
16	15	89	40.899	1556	1404	0.025	35.02	1.37	38.90	11
17	15	89	45.200	1637	1507	0.02	31.12	1.13	34.38	10
18	15	89	45.300	1696	1539	0.02	34.64	1.65	37.31	8
19	15	89	48.400	1288	1198	0.01	12.36	41.06	12.88	4
20	16	58	23.399	957	901	0.01	10.21	4.72	10.53	3
21	16	58	22.301	930	872	0.01	11.73	2.71	12.09	3
22	16	58	29.501	1024	957	0.01	13.36	2.73	14.34	7
23	16	58	22.301	717	681	0.01	5.27	28.05	5.74	9
24	19	70	24.800	980	930	0.02	15.59	7.02	16.66	7
25	19	70	25.401	1046	945	0.02	19.39	3.92	20.92	8
26	19	70	27.099	1131	999	0.025	26.01	2.97	28.28	9
27	33	80	18.501	782	761	0.01	4.11	6.27	3.91	5
28	33	80	16.000	788	752	0.01	6.38	7.25	6.30	1
29	33	80	19.199	854	825	0.01	5.52	5.03	5.98	8
30	33	80	35.100	1369	1260	0.01	13.79	46.58	15.06	9

*In theory, this difference should be zero. So, smaller this error, better is the accuracy of Fit.

or

$$Q = \{\text{slope of the ln H vs .1/T plot at a constant } (-\dot{H}/H)\text{value}\}.R.N \quad (15)$$

4. Results and discussion

4.1. New results

The average relative density, ρ_{av}, of the 8 compacts varied from 58 to 94% and the average grain size, L, from 11 nm to 62 nm. In each compact, the microhardness was measured at different locations. As machine outputs, the maximum microhardness value, H_{max}, in a given test and the corresponding value of E were obtained. The results are presented in Table I.

As H, E and ρ are directly related [21], it was concluded, consistent with the earlier findings [22, 23], that the local density in a compact changed from one location to the next. A careful examination revealed the following.

(a) Sometimes the compact had a reasonably uniform density in its entire volume, which was close to the average relative density of the compact (see Fig. 3a corresponding to a compact of $\rho_{av} = 58\%$ and Table I).
(b) Occasionally, because of the accidental choice of sites, the local densities were close to each other but they were clearly different from the ρ_{av} value of the compact (see Fig. 3b from a compact of $\rho_{av} = 89\%$ and Table I).
(c) In some cases the local densities differed widely and were also clearly different from the average density of the compact (see data in Table I pertaining to the compact with $\rho_{av} = 90\%$).

The results reveal (i) that nanocrystalline compacts are highly non-uniform with regard to the local mechanical response, and (ii) that depending on the location selected for a microhardness measurement, the local response may be close to or vastly different from the average response one would obtain by subjecting the entire specimen to a macro-measurement. In this view, the earlier finding [22, 23] that in a Pd compact the microhardness varied between 2.2 and 4.3 GPa is attributable to the local variations in the density of the compact. The other finding [22, 23] that spatial variation in the microhardness of n-Pd compacts was more than in n-Cu compacts is traced to the nature of the neighbourhood randomly chosen for the microhardness measurements. It is also conceivable that in those experiments compaction was more uniform in n-Cu than in n-Pd.

For the 30 experimental conditions listed in Table I, H-t ($t \leq 50$ s) combinations were directly obtained from the microhardness tester. It was verified that Equation 11 was satisfied at all the 30 locations. Fig. 4 displays some results.

From the raw H-t data and Equation 5, the H vs. $(-\dot{H}/H)$ relationship was obtained for all the 30 experimental sites in the 8 compacts. Fig. 5 presents three representative examples. In all the 30 cases, the H (which is proportional to the uniaxial yield stress) vs. $(-\dot{H}/H)$ (which is proportional to the corresponding strain rate) relationship was linear over the nearly two orders of magnitude change in strain rate present in a microhardness test. That is, the slope of these plots and hence the strain rate sensitivity index, m (=1/N), remained constant during every microhardness test, which validates the assumption made in the

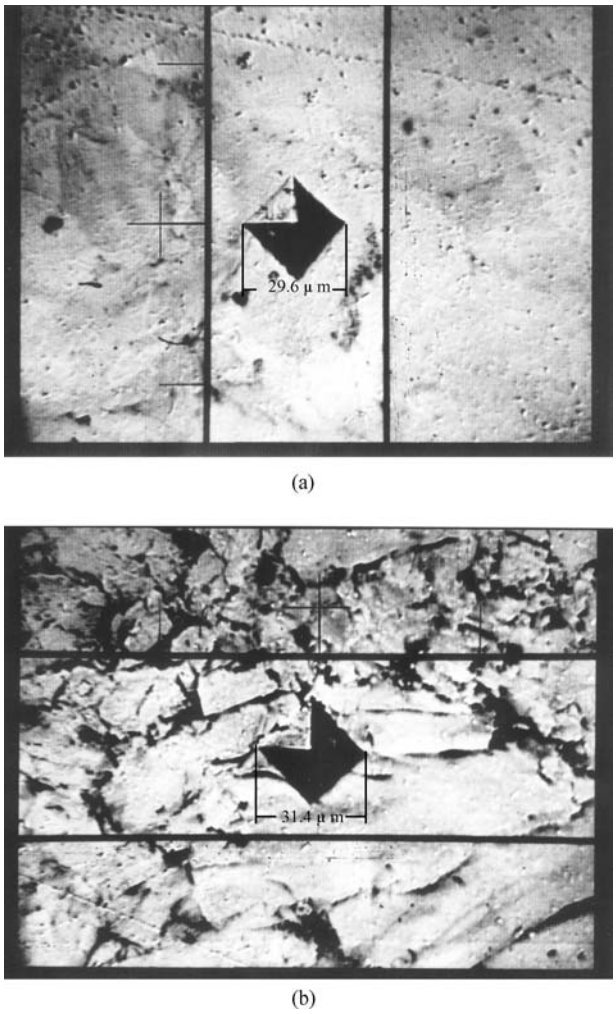

Figure 3 Micrographs indicating microindentations and their characteristic surroundings in: (a) a Pd compact of average relative density 58% (b) a Pd compact of average relative density 89%.

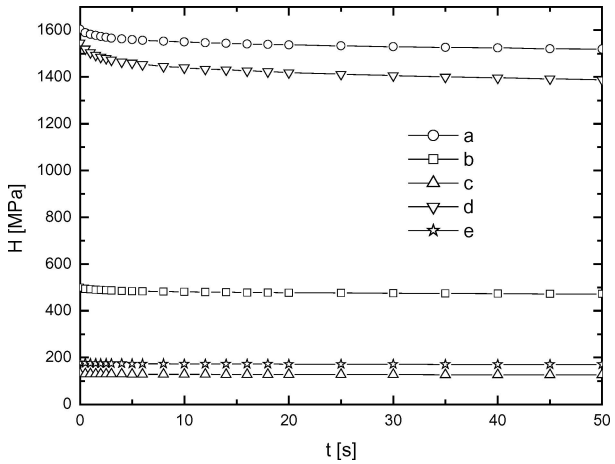

Figure 4 H-t relationship. Symbols represent experimental points. Full curves are predictions based on Equation 11. Compacts of: (a) $\rho_{av} = 94\%$, (b)–(c) $\rho_{av} = 90\%$, (d)–(e) $\rho_{av} = 71\%$.

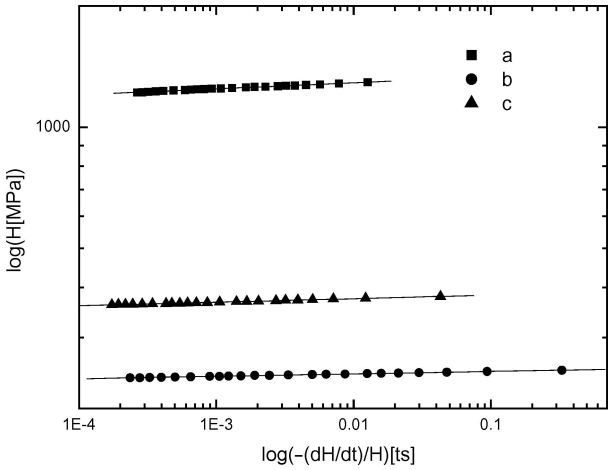

Figure 5 $H - [-(\frac{\dot{H}}{H})]$ plots derived from curves similar to those presented in Fig 4. H is proportional to the uniaxial flow stress; $[-(\frac{\dot{H}}{H})]$ is proportional to the corresponding strain rate. (a) $\rho_{av} = 94\%$, (b) $\rho_{av} = 90\%$, (c) $\rho_{av} = 71\%$.

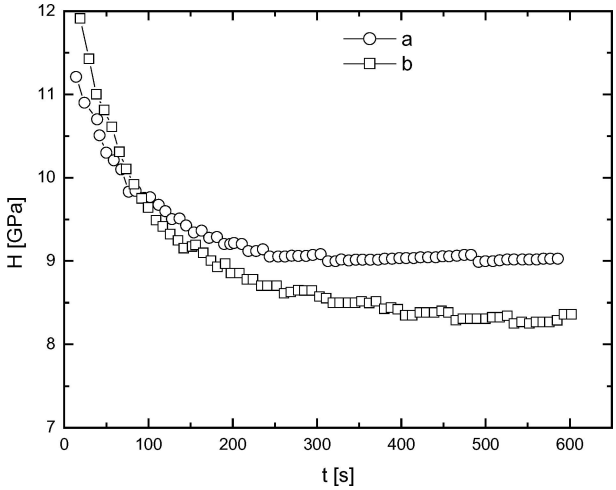

Figure 6 *H-t* relationship: (a) a Fe-63 vol% TiN composite of average grain size 12 nm, tested at 573 K; (b) a Ni-58 vol% TiN composite of average grain size 10 nm, tested at 598 K. Full curves are predictions based on Equation 11. Symbols represent experimental data given in ref. [12].

analysis that N has a constant value in a microhardness test. In the present experiments m varied between 0.01 and 0.025, i.e., the values lay in the range commonly encountered during creep. A, B, m, $(H_{max} \cdot m)$ and the percentage difference between the values of A and $(H_{max} \cdot m)$ (which should be zero according to the analysis) were obtained using figures similar to Figs 4 and 5 and Equations 5 and 11. These findings are also included in Table I.

From Table I and the earlier results [22, 23], it is clear that microhardness can vary significantly in a given compact from one location to the next and that it is not easy to assign a mean microhardness value corresponding to a mean compact density, ρ_{av}.

4.2. Results of Ogino *et al.* [12]

Ogino *et al.* [12] have plotted *H-t* experimental curves at different temperatures for Fe-63 vol% TiN and Ni-58 vol% TiN nanocomposites (Fig. 6 of ref. [12] covering a time interval of 600 s). From these data it is possible to validate Equation 11 and obtain the activation energy for the rate controlling deformation process (Equation 15).

Equation 11 was obeyed at all temperatures in case of both the composites. Fig. 6 displays an example each for the two composites. As before, the $\log H - \log(-\dot{H}/H)$ relationship could be obtained for both the materials at all temperatures. Fig. 7 displays these plots. The following observations are in order.

(a) In these tests, the strain rate varied by an order of magnitude during a microhardness test.

(b) Although m was constant in a test, its magnitude depended on the test temperature, particularly in the Fe-63 vol% TiN composite. But the variation was not systematic. And so, the scatter was attributed to experimental errors. As a result, for each material the average value of m (the mean value of m in the temperature interval) was used to calculate the activation energy for the rate controlling flow process.

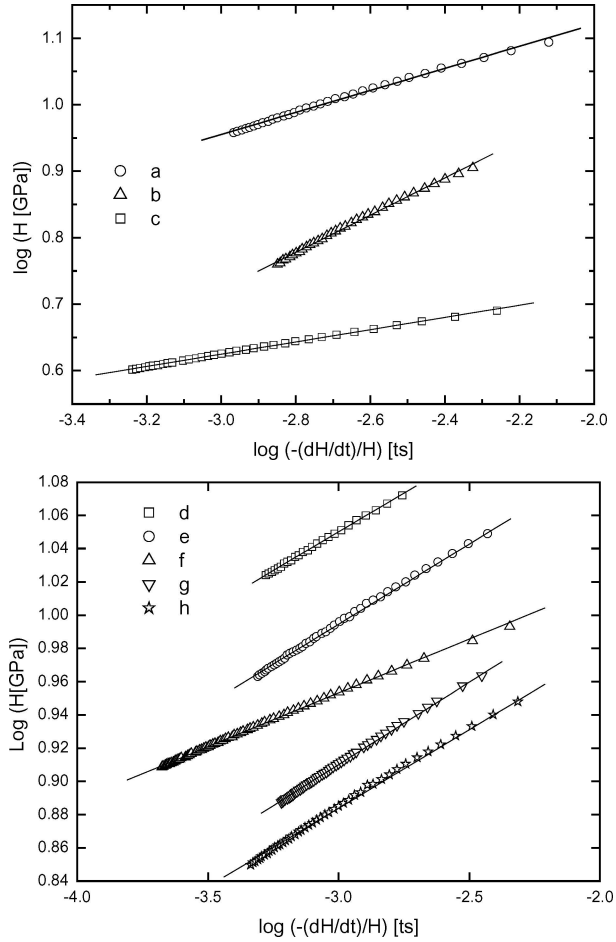

Figure 7 $H - [-(\frac{\dot{H}}{H})]$ plots derived from curves similar to those presented in Fig 6. H is proportional to the uniaxial flow stress; $[-(\frac{\dot{H}}{H})]$ is proportional to the corresponding strain rate. (a)–(c) A Fe-63 vol% TiN composite of average grain size 12 nm, tested respectively at 573, 673 and 773 K; (d)–(h) A Ni-58 vol% TiN composite of average grain size 10 nm, tested respectively at 573, 578, 633, 648 and 673 K. Experimental points are after ref. [12].

In Figs 8 and 9 the activation energy for the rate controlling deformation process is obtained for the two materials by plotting log H against $1/T$ at a fixed value of $\log(-\dot{H}/H)$ and using Equation 15. The activation energy, Q, for the Fe-63 vol% TiN composite was 82 kJ mol^{-1}. Q for the Ni-58 vol% TiN composite was 140 kJ mol^{-1}. These values are realistic, because for a host of materials the activation energy for creep deformation has been reported to be of the order of 0.2–0.7 times the activation energy for self diffusion of the major elements that constitute the material [24]. The activation energy for self diffusion in α-Fe is 250–280 kJ mol^{-1}, in α-Ti it is 170 kJ mol^{-1} and in Ni it is 277–400 kJ mol^{-1}.

The data analysed in this paper pertain to compacts prepared by consolidation. The average relative density of the compacts varied between 58 and 94%. Ogino *et al*. [12] have not reported the relative density of the compacts used by them. Based on the present results, it is reasonable to suggest that in the range of average relative densities considered, the relationship governing the time variation of microhardness was similar to that reported for power law creep in fully dense solids. Also the relationship was unchanged when the duration of measurement was increased from less than 50 s to about 600 s.

In a future study the time dependent variation of microhardness of compacts of nearly 100% relative density, e.g., prepared by electro-deposition, will be investigated. It is likely that while the relationship will be the same, the rate of deformation will be different. It is known from the powder metallurgy literature concerning microcrystalline materials [8–11, 25] that both Young's modulus and Poisson's ratio change with density and these elastic constants significantly affect the flow behaviour.

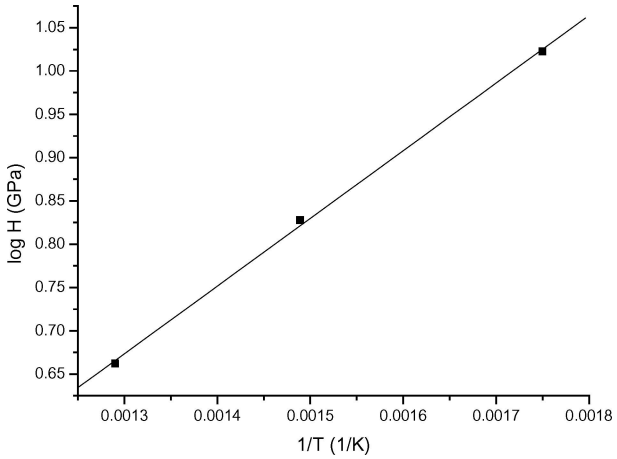

Figure 8 Arrhenius plot for the Fe-63 vol% TiN composite at a constant $\log[-(\frac{\dot{H}}{H})]$ value of 2.6.

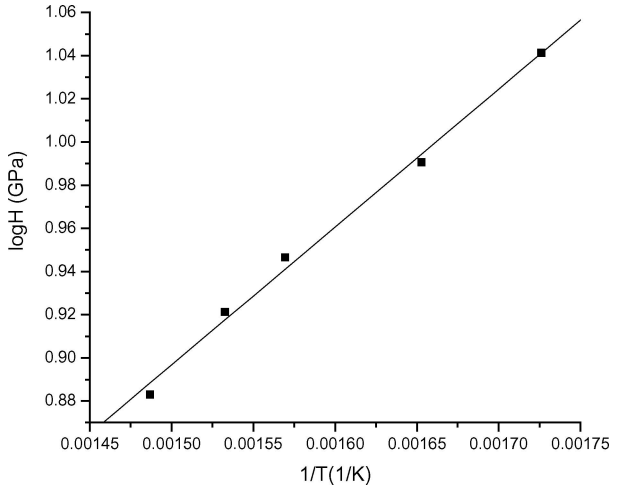

Figure 9. Arrhenius plot for the Ni-58 vol% TiN composite at a constant $\log[-(\frac{\dot{H}}{H})]$ value of 3.0.

5. Conclusions

The following conclusions could be drawn from this investigation.

1. Spatial variation in the microhardness of a compact can be large due to differences in density at different locations. Therefore, assigning a microhardness value for a compact of a given average relative density will have to be done with caution.
2. In *n*-Pd compacts of average relative density that ranged between 58 and 94%, the hardness value and Young's modulus were directly related.
3. When creep effects are significant, as in the present experiments on porous n-Pd compacts and those of Ogino *et al*. [12] on Fe-63 vol% TiN and Ni-58 vol% TiN nanocomposites tested at elevated temperatures, the microhardness, H, varies with time, t, as $H \approx H_{\max} - A\ln(Bt+1)$, where $H_{\max}$ is the maximum hardness measured in a microhardness test, A $(=H_{\max}.m)$ and B are constants and m is the strain rate sensitivity index. This expression contains a single fitting parameter, B. This equation holds good for both small and large times of load application in a microhardness test.
4. The relation $\dot{\varepsilon} = K_1\sigma^N$ ($\dot{\varepsilon}$ = uniaxial strain rate, σ = the corresponding stress, $N = 1/m$ = constant and K_1 = constant) or its analogous version $(-\dot{H}/H) = C_4H^N$ (H = hardness, $\dot{H}$= its time derivative, C_4 = constant) was obeyed in all the micro-indentation tests reported here.
5. The values of the true activation energy for the rate controlling process in the deformation of nanocrystalline Fe-63 vol% TiN and Ni-58 vol% TiN composites by micro-indentation were 82 and 140 kJ mol^{-1} respectively.

Acknowledgments

KAP thanks the Alexander von Humboldt-Stiftung, Bonn and the Institute of Nanotechnology, FZK, Karlsruhe, Germany, for financial support. The authors are grateful to Prof H. Gleiter for a critical review of the manuscript.

References

1. H. HAHN and K. A. PADMANABHAN, *Nanostr. Mater.* **6** (1995) 191.

2. *Idem*., in "Advanced Materials and Processing," edited by K. S. Shin, J. K. Yoon and S. J. Kim, (Korean Inst. of Metals and Mater., Kyongju, Korea, 1995) Vol. 3, p. 2119.
3. K. A. PADMANABHAN and H. HAHN, in "Synthesis and Processing of Nanocrystalline Powder," edited by G. Burrell, (Minerals, Metals and Mater. Soc., Warrendale, PA, USA, 1996) p. 21.
4. D. G. MORRIS, "Mechanical Behavior of Nanostructured Materials," (Mater. Sci. Foundations 2, Trans. Tech. Publ., Aedermannsdorf, Switzerland, 1998) p. 1.
5. K. A. PADMANABHAN, *Mater. Sci. Eng.* **A304–306** (2001) 200.
6. K. S. KUMAR, H. VAN SWYGENHOVEN and S. SURESH, *Acta Mater.* **51** (2003) 5743.
7. A. J. KOZLOV, D. H. KIM, A. YEZERETS, P. ANDERSEN, H. H. KUNG and M. C. KUNG, *J. Catal.* **209** (2002) 417.
8. T. J. WEBSTER, R. W. SIEGEL and R. BIZIOS, *Nanostr. Mater.* **12** (1999) 983.
9. G. D. MCADAM, *J. Iron Steel Inst.* **68** (1951) 346.
10. G. ARTUSIA, V. GALLINA, G. MANNONE and E. SGAMBETTERA, *Powder Met.* **9** (1966) 89.
11. R. HAYNES and J. T. EGEDIEGE, *ibid.* **32** (1989) 47.
12. Y. OGINO, T. YAMASAKI and B. L. SHEN, in "Advanced Materials and Processing," edited by K. S. SHIN, J. K. YOON and S. J. KIM (Korean Inst. of Metals and Mater., Kyongju, Korea, 1995) Vol. 3, p. 2149.
13. W. M. YIN, S. H. WHONG, R. MIRSHAMS and C. H. XIAO, *Mater. Sci. Eng.* **A301** (2001) 18.
14. H. IWASAKI, K. HIGASHI and T. G. NIEH, *Scr. Mater.* **50** (2004) 395.
15. A. HASNAOUI, H. VAN SWYGENHOVEN and P. M. DERLET, *Acta Mater.* **50** (2002) 3927.
16. R. BIRRINGER, H. GLEITER, H.-P. KLEIN and P. MARQUARDT, *Phys. Lett.* **102A** (1984) 461.
17. H. P. KLUG and L. E. ALEXANDER, "X-Ray Diffraction Procedures for Polycrystalline and Amorphous Materials" (John Wiley, New York, 1954).
18. J. WEISSMUELLER, J. LÖFFLER and M. KLEBER, *Nanostr. Mater.* **6** (1995) 105.
19. W. B. LI, J. L. HENSHALL, R. M. HOOPER and K. E. EASTERLING, *Acta Metall. Mater.* **39** (1991) 3099.
20. K. A. PADMANABHAN, R. A. VASIN and F. U. ENIKEEV, "Superplastic Flow: Phenomenology and Mechanics" (Springer Verlag, Heidelberg-Berlin, 2001).
21. S. VEPREK, *Thin Solid Films* **297** (1997) 145.
22. G. W. NIEMAN, J. R. WEERTMAN and R. W. SIEGEL, *Scr. Metall. Mater.* **24** (1990) 145.
23. *Idem*., *J. Mater. Res.* **6** (1991) 1012.
24. J. H. GITTUS, "Creep, Viscoelasticity and Creep Fracture in Solids" (Applied Science, London, 1975) pp. 168–171, 182–185, 192–193, 196–197, 278–279, 342–343, 396–399, 500–501, 526–527, 538–539, 542–547, 638–639.
25. H. A. KUHN, in "Powder Metallurgy Processing," edited by H. A. KUHN and A. LAWLEY, (Academic Press, New York, 1978) p. 99.

Received 9 August 2004
and accepted 6 May 2005